A 2.4 GHz Differential Wavelet Generator in 0.18 μm Complementary Metal–Oxide–Semiconductor for 1.4 Gbps Ultra-Wideband Impulse Radio in Wireless Inter/Intra-Chip Data Communication

Pran Kanai SAHA[*], Nobuo SASAKI, Kentaro KIMOTO and Takamaro KIKKAWA[†]

Research Center for Nanodevices and Systems, Hiroshima University, 1-4-2 Kagamiyama, Higashi-Hiroshima, Hiroshima 739-8527, Japan

Ultra-wideband impulse based radio systems use Gaussian monocycle pulses as transmitted signals at the transmitting end and as template signals at the receiving end. In this paper we present a new fully integrated differential Gaussian monocycle pulse generator in 0.18 μm complementary metal–oxide–semiconductor (CMOS) technology. Here the Gaussian monocycle pulse is generated from triangular shaped pulse by a single differentiator circuit and it is then converted into differential form by using a single input to dual output amplifier. The developed circuit occupies a small area of 0.06 mm^2 and consumes a total power of 44 mW at 1.8 V. The transmission of the generated differential Gaussian monocycle pulse at a rate of 1.4 Gbps through integrated dipole antenna in the same Si-substrate for intrachip communication in future ultralarge scale integrated circuit (ULSI) is verified by simulation and results are presented here.   [DOI: 10.1143/JJAP.45.3279]

1. Introduction

To meet the challenge of three-dimensional (3D)-integration in future ultralarge scale integrated circuit (ULSI), wireless inter/intra-chip communication has been developed using capacitive and inductive coupling technologies[1,2] but for both techniques the communication distance is limited to 300 μm, and the system has no multi-chip accessibility. To overcome these problems, global wireless interconnection, which uses electromagnetic wave transmission by an integrated antenna[3] and ultra-wideband (UWB) transceiver system has been proposed as shown in Fig. 1. Among the different techniques for UWB systems, such as direct sequence spread spectrum (DSSS),[4] time-hopping spread spectrum (TH-SS),[5] and frequency-hopping spread spectrum (FH-SS),[4] impulse radio-based UWB uses very short Gaussian monocycle pulses (GMP) which have wide bandwidth to achieve spread spectrum transmission.[5] The GMP's spectrum does not contain low frequency components, including dc, that are found in other UWB pulses such as step and Gaussian. Since GMP transmission does not require any carrier, the transceiver circuit is simple and occupies a small area, as it does not require any complex frequency recovery system at the receiver end. In view of the above merits, impulse-based UWB technology can be effectively used in wireless inter/intra-chip data communication for future ULSI. However, the on-chip generation of short GMPs is the major obstacle for the intended application of impulse based UWB technology.

The generation of GMP wavelets using step recovery diode (SRD) based circuits for this application is not acceptable because of the difficulties of SRD integration in complementary metal–oxide–semiconductor (CMOS) technology.[6] Moreover, the charging and discharging time of SRDs limit the pulse repetition rate, which results in a low data transmission rate. Generation of GMP by the resist-
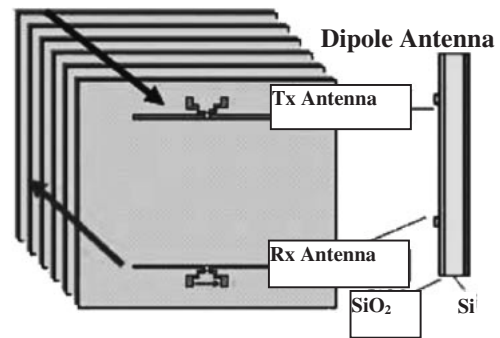
ance–inductance–capacitor (RLC) network along with a pass transistor in CMOS has been reported in ref. 7, but it occupies a large area because of the use of inductance. However, the use of the technique described to generate GMP is applied at the cost of Si-area, which is not desirable for the intended application.

This work focuses on the implementation of a differential Gaussian monocycle pulse generator (DGMP) in CMOS technology which is inductor-less, low complexity, occupies a small area, and thus is low cost.

The paper is organized as follows. Section 2 contains the GMP generation principle. Section 3 describes the operation of DGMP circuits. HSPICE simulation results for the circuit are described in §4. Transmission and reception of DGMP pulse trains using integrated dipole antenna pairs in the same standard Si substrate are reported in §5. Concluding remarks are given in §6.

2. Gaussian Monocycle Pulse Generation

Typically a differentiator generates two impulses at the rising and falling edges of the differentiator's input when the input is a rectangular pulse as shown in Fig. 2(a). Figure 2(b) depicts the generated impulses. The interval between the two impulses depends on the rectangular pulse duration (t_d). If the duration (t_d) is reduced, the negative

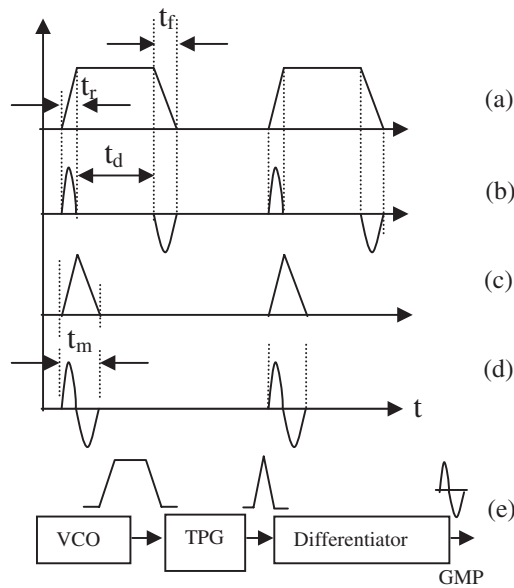Fig. 1. Intra/interchip wireless interconnect system for future ULSI.

Fig. 2. Generation of Gaussian monocycle pulse. (a) Rectangular pulse. (b) Gaussian impulse. (c) TP. (d) GMP. (e) GMP generation schematic.

impulse shifts to the left until it coincides with the end of the positive impulse, and this forms the Gaussian monocycle pulse (GMP). If t_d equals zero, then the rectangular pulse becomes a triangular pulse (TP) with Gaussian properties. The TP and GMP are shown in Figs. 2(c) and 2(d), respectively. The GMP generation schematic is shown in Fig. 2(e). Here a triangular pulse generation (TPG) circuit generates a TP from the rectangular shaped pulse which is the voltage controlled oscillator (VCO) output. The differentiator then converts the TP into the GMP. The detailed circuit descriptions are given in the next section. The GMP's duration (t_m) depends on the rising (t_r) and falling (t_f) times of the triangular pulse and is given by $t_m = t_r + t_f$. The GMP center frequency (f_c) is the reciprocal of t_m. In this study, this technique has been implemented in a CMOS circuit to generate differential GMP wavelets for the impulse based UWB transceiver. A schematic block diagram of the differential GMP circuit developed is shown in Fig. 3. The resistance–capacitor (RC) network shown in Fig. 3 is used as the differentiator in the 2.4 GHz frequency range of interest. The transfer function [G(s)] in the s-domain of the RC network is given as

$$G(s) = \frac{v_{\text{GMP}}}{v_{\text{triang}}} = \frac{RCs}{1 + RCs} \tag{1}$$

where $s = j\omega = d/dt$, v_{triang} = the triangular pulse as differentiator input, and v_{GMP} = the differentiator output (Gaussian monocycle pulse).

Considering $RCs \ll 1$, eq. (1) can be written as

$$v_{\text{GMP}} = T_c \frac{dv_{\text{triang}}}{dt} \tag{2}$$

where T_c = derivative time coefficients = RC. Equation (2) represents the output of an ideal differentiator. Thus the RC values are chosen in such a way that the network acts almost as an ideal differentiator to generate GMPs from triangular shaped pulses.

3. DGMP Circuit

The VCO generates a differential clock signal. The VCO circuit consists of three stages, two single-ended ring oscillators coupled together by weak inverters that keep the two structures 180° out of phase. This structure somewhat reduces the sensitivity to supply and substrate noise while enjoying the benefits of differential oscillators. Figures 4(a) and 4(b) show a three-stage ring oscillator and the differential delay cell, respectively. The VCO frequency is controlled by the control voltage (V_{c1}) shown in Fig. 4(b). The triangular shaped pulse is then generated from the VCO output using a digital pulse shaping circuit which consists of a voltage controlled non-inverting delay circuit, exclusive-or (XOR) gate, and AND gate. The formation of the triangular pulse is shown in Fig. 5. The delay circuit shifts the rectangular shaped pulse by a time which is slightly less than the rise time of the VCO output. The delay time is controlled by the control voltage (V_{c2}). The triangular pulse generation circuit is shown in Fig. 6. The triangular pulse is then differentiated to generate the GMP. The differentiator (shown in Fig. 3) is designed using metal-insulator-metal capacitor (MIMCAP) and poly resistor (R) in such a way that it behaves close to an ideal differentiator in the frequency range of interest. The amplitude of the GMP depends on the derivative time constant (RC), t_r, and t_f. To reduce the common mode noise and transmit the GMP by integrated dipole antenna, the single-ended GMP is converted into a differential GMP (DGMP) using a single-input differential-output (SIDO) amplifier. Figure 7 shows the
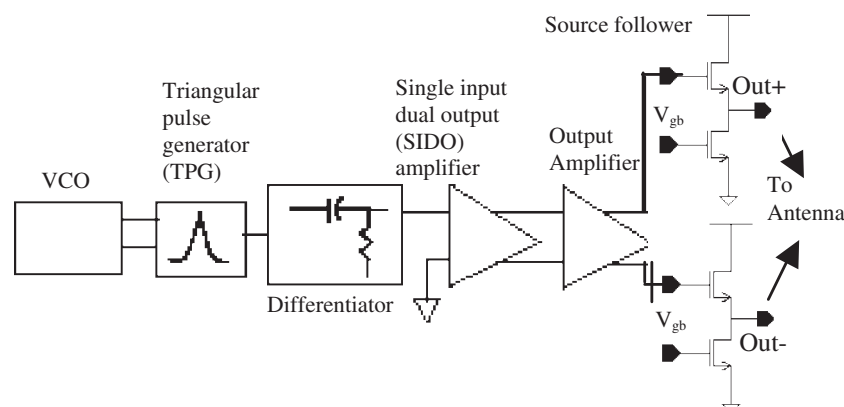

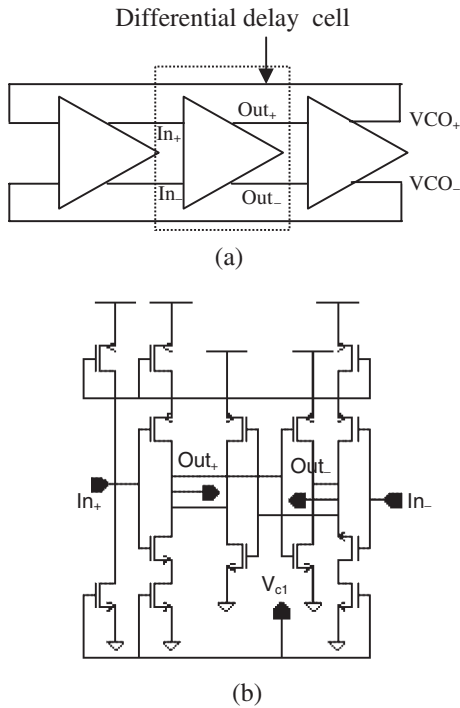Fig. 3. Schematic block diagram of a DGMP wavelet generator.

(a)

(b)

Fig. 4. Differential VCO. (a) Three-stage ring oscillator. (b) Differential delay cell.
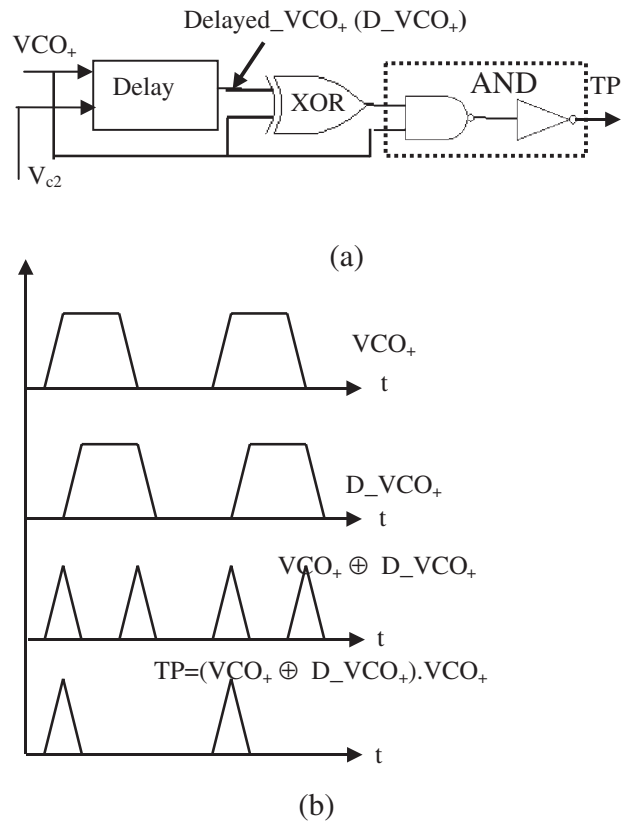

(a)

(b)

Fig. 5. Formation of triangular pulse. (a) TP generation schematic. (b) TP generation step from rectangular shaped pulse having finite rise and fall times.

DGMP generation circuit. The SIDO is a CMOS differential amplifier circuit consisting of nMOS current source and pMOS load resistors as shown in Fig. 7. The size of the pMOS load resistors is chosen in such a way that the drain current of the driver transistors M1 and M2 as shown in Fig. 7 are almost equal, so that the differential output can be obtained from the SIDO circuit even though one input of the SIDO is grounded. The DGMP is further amplified by an output amplifier. The output amplifier architecture is the same as the SIDO. The amplifier gain is adjusted by optimizing the size of the driver transistors (M3 and M4) and the size of the pMOS (M5 and M6) load resistors as shown in Fig. 7. A source follower circuit (shown in Fig. 3) is used to avoid reflection due to impedance mismatch between the DGMP circuit and the transmitting antenna.

4. Results of Simulation and Discussion

The circuit is implemented in a 0.18-μm CMOS process. The circuit layout is shown in Fig. 8. The "HSPICE"[8])
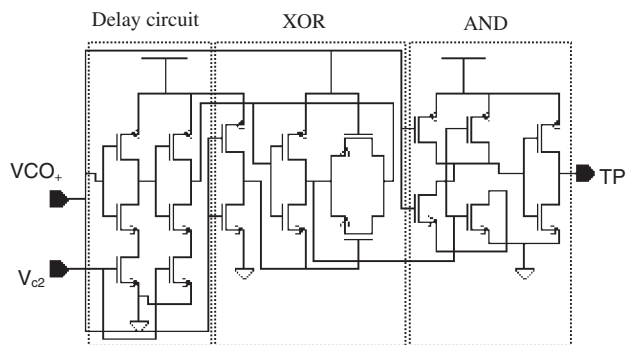

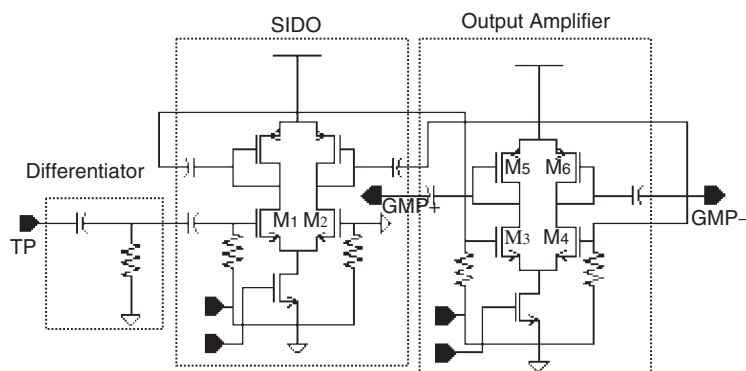Fig. 6. Triangular pulse generation circuit.
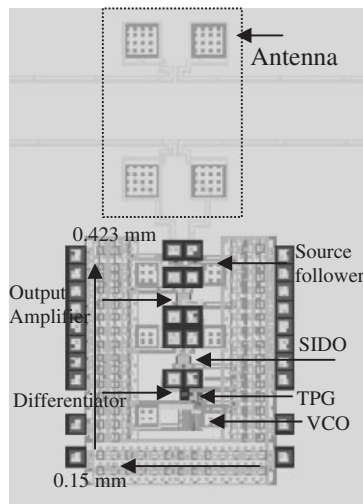

Fig. 7. DGMP generation circuit.

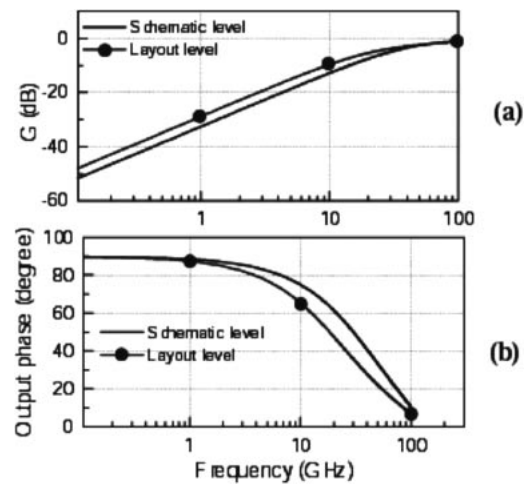Fig. 8.   Chip layout (antenna size is not to scale).

Fig. 10.   Frequency response of differentiator. (a) Gain vs frequency. (b) Output phase vs frequency.
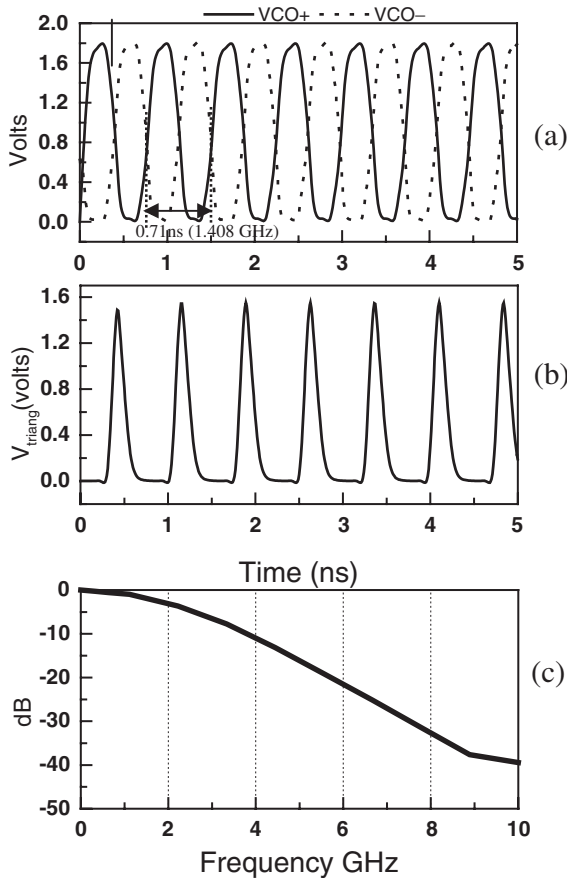

Fig. 9.   Generation of triangular pulse from VCO output. (a) VCO output. (b) TP. (c) FFT of TP.

netlist is created from the chip layout using the Calibre™ parameter extraction program. The simulation is then carried out with the extracted netlist using the well-known simulation program "HSPICE". All parasitic resistance, capacitance, and coupling capacitance are taken into account during the simulation. The simulation shows that the differential VCO first generates a rectangular shaped pulse having a finite rise time of 0.185 ns and a fall time of 0.210 ns. Figure 9(a) shows that the highest frequency of the

VCO is 1.408 GHz at a control voltage of 1.8 V. The phase noise for a 1 MHz offset is -95.47 dBc/Hz. The delay circuit shifts the rectangular shaped pulse by a time which is slightly less than the rise time (0.185 ns) of the VCO output. The triangular shaped pulse with a rise time of 0.120 ns and fall time of 0.239 ns is generated as shown in Fig. 9(b) from the VCO output. The fast Fourier transform (FFT) of the TP shown in Fig. 9(c) confirms that the generated TP has the same characteristics as a Gaussian impulse. Figures 10(a) and 10(b) show gain vs frequency of the differentiator and output phase vs frequency. The frequency response of the RC network for generating a GMP from a TP shows that the RC network acts as differentiator at frequencies below 12 GHz [refer to Fig. 10(a)], and the phase of the differentiator at a frequency of 2.4 GHz is 84°, which is only 6° below that of an ideal differentiator. This performance is due to the parasitic effect of the MIMCAP. The GMP generated from TP using the differentiator from the simulation is shown in Fig. 11(a). The amplitude of the negative impulse of the GMP is half of that of the positive impulse because the fall time t_f (0.239 ns) of the TP is twice the rise time t_r (0.120 ns) of the TP. The pulse width of the GMP is 0.41 ns, which is slightly higher than that of $t_r + t_f$, because of the long falling tail of the TP, which arises due to the loading effects of the differentiator on the TP generating circuit. The FFT of GMP shown in Fig. 11(b) depicts that the GMP has a center frequency (f_c) of 2.4 GHz and a 3-dB bandwidth of 2.8 GHz. However, further increasing f_c is possible by generating a fast rising and falling edge of the triangular pulse. The differential Gaussian monocycle (DGMP) generated by the SIDO circuit is shown in Fig. 12(a). Figure 12(a) shows that the DGMP peak-to-peak amplitude level is lower than that of the GMP. Because one input of the SIDO amplifier circuit is grounded, no amplification is done by the SIDO circuit. The DGMP is amplified by the output amplifier (shown in Fig. 7). The output amplifier has a voltage gain (A_v) of 2.31 (7.28 dB) at the center frequency of the GMP (2.4 GHz) and a wide bandwidth as shown in Fig. 12(b). The amplified DGMP is shown in Fig. 12(c). Figure 12(c) shows that the DGMP is amplified 1.8 times the SIDO output, which is lower than the voltage gain of the

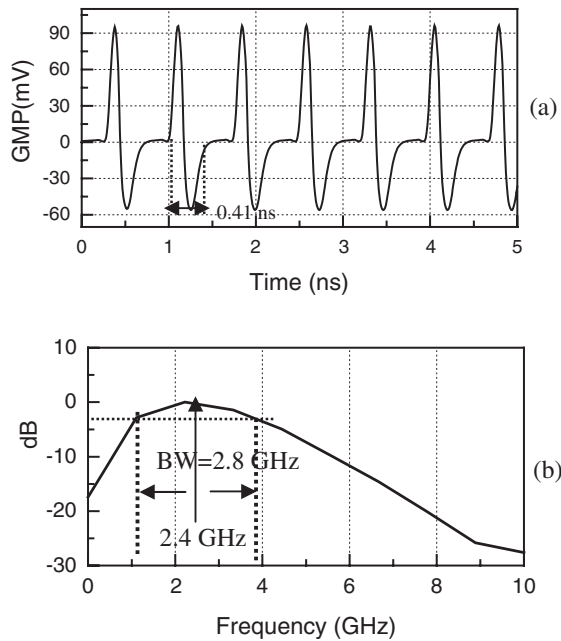Jpn. J. Appl. Phys., Vol. 45, No. 4B (2006)

P. K. SAHA *et al.*

Fig. 11. Generation of GMP from TP. (a) Single ended GMP. (b) FFT of GMP.
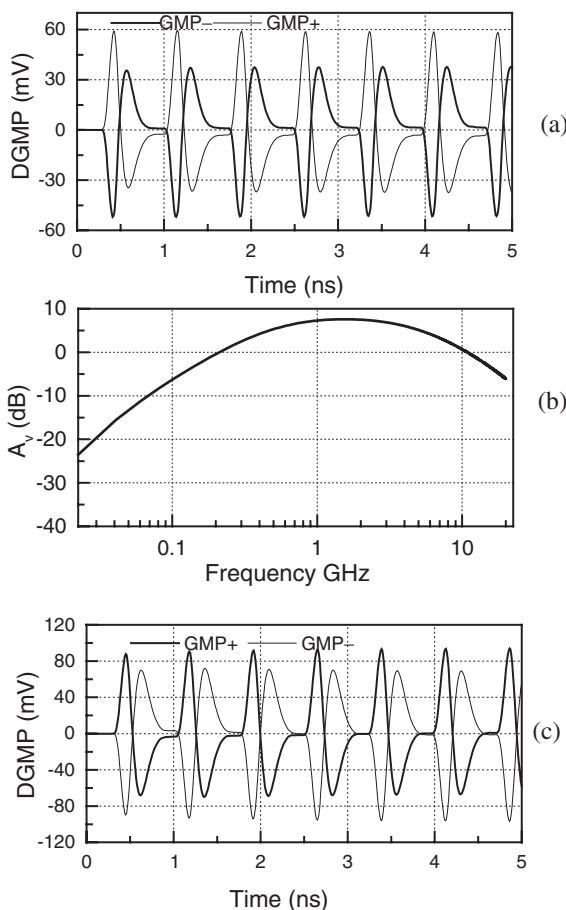

Fig. 12. Generation of DGMP from GMP. (a) SIDO converter output. (b) Voltage gain (A_v) of output amplifier vs frequency. (c) DGMP after output amplifier.

output amplifier. This occurs because of the voltage drop in the dc blocking capacitor used between the output amplifier and the source follower circuit. The amplified DGMP is then

transmitted by a transmitting antenna through the source follower circuit.

5. GMP Transmission/Reception

A pair of dipole antennas 6 mm long, 10 μm wide, and 1 μm thick on a 10 Ω cm standard Si substrate are used to verify the DGMP transmission in intrachip data communication. Characteristics (*S*-parameters) of this 6-mm-long dipole antenna pair on a silicon substrate were evaluated by MW Studio[9] and were then verified by measurement.[10] The verified *S*-parameters are used to generate the HSPICE netlist macromodel using an EMtoSPICE™ converter.[11] The accuracy of the macromodel generated was verified by comparing the *S*-parameter obtained from the HSPICE simulation with that obtained from the MW studio simulation as shown in Fig. 13. Figure 13 shows that the antenna characteristics in both simulations are very close to each other. The antenna's resonance frequency is the same as that obtained from the MW studio simulation. Thus it can be concluded that the HSPICE macromodel generated by the EMtoSPICE™ converter provides accurate transmission and reception characteristics of the integrated dipole antenna pair in the Si substrate.

The antenna input impedance (Z_{in}) is computed from the S_{11} parameter using the following equation:

$$Z_{in} = Z_0 \frac{1 + S_{11}}{1 - S_{11}} \tag{3}$$

where Z_0 = reference impedance = 100 Ω.

From eq. (3) the $|Z_{in}|$ of the 6-mm-long dipole antenna in the Si substrate at 2.4 GHz is 210 Ω. The output impedance of the source follower circuit is computed from the small signal analysis of the circuit and is 41 Ω at 2.4 GHz. Since the antenna input impedance is higher than the source follower output impedance, no ringing occurs during the DGMP transmission by the integrated dipole antenna.

To confirm the transmission and reception of GMP by the integrated antenna in silicon, a simulation is carried out on the DGMP circuit including the source follower layout extracted netlist and the HSPICE macromodel of the integrated antenna pairs. The simulated results for different communication distances (*d*, 1–3 mm) are shown in Fig. 14. Figure 14(a) shows that the transmitted signal amplitude level is half that of the DGMP because the voltage gain of the source follower circuit is 0.5 (−6 dB). Figures 14(b) and 14(c) show that the received signal is the derivative of the transmitted signal due to the antenna effect. The received signal level decreases with increasing separation distance (*d*), which is expected. Figure 14 shows that transmission and reception is achieved at a rate of 1.4 GHz. Thus, a maximum data transmission rate of 1.4 Gbps could be achieved.

The performance is summarized in Table I.

6. Conclusions

The architecture for 2.4 GHz DGMP generation in an 0.18-μm CMOS process for a UWB impulse-based radio system for wireless inter/intra-chip data communication is developed. The DGMP generation circuit developed occupies a small area (0.06 mm²) and consumes a total power of 44 mW in the transmit mode from a 1.8 V supply. Trans-
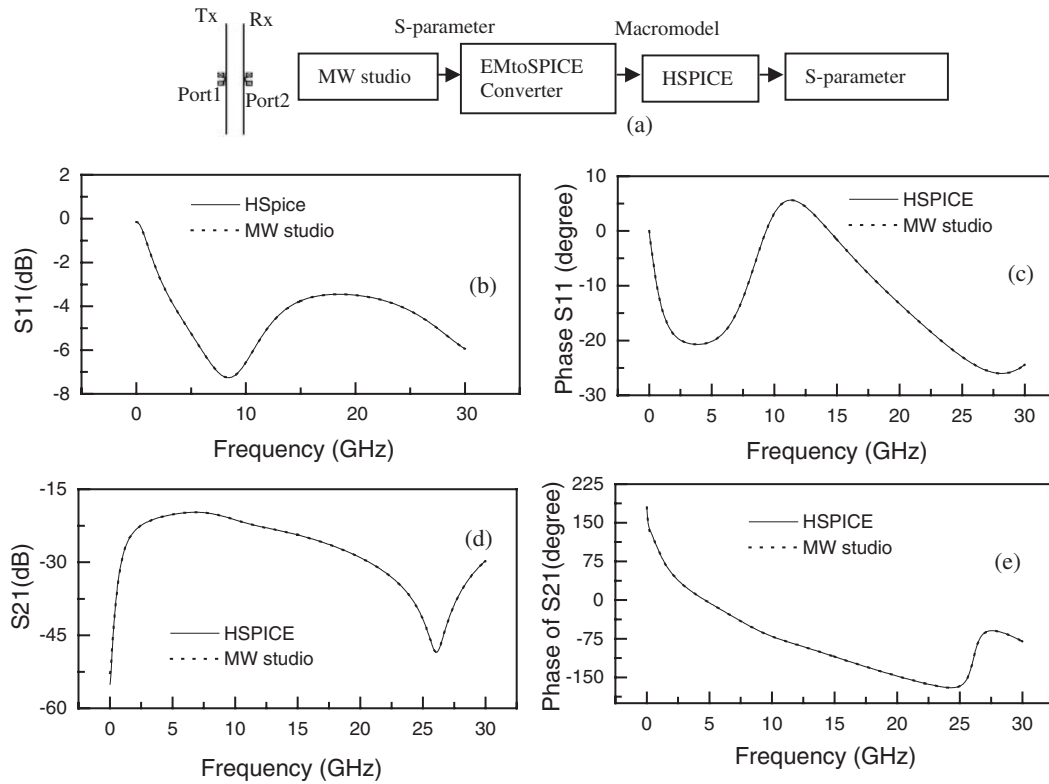
Fig. 13. Comparison of the *S*-parameters of the antenna pair obtained from MW studio and those from the HSPICE macromodel for $d = 1$ mm. (a) Generation of macromodel. (b) Magnitude of reflection co-efficient (S_{11}). (c) Phase of S_{11}. (d) Magnitude of transmission co-efficient (S_{21}). (e) Phase of S_{21}.
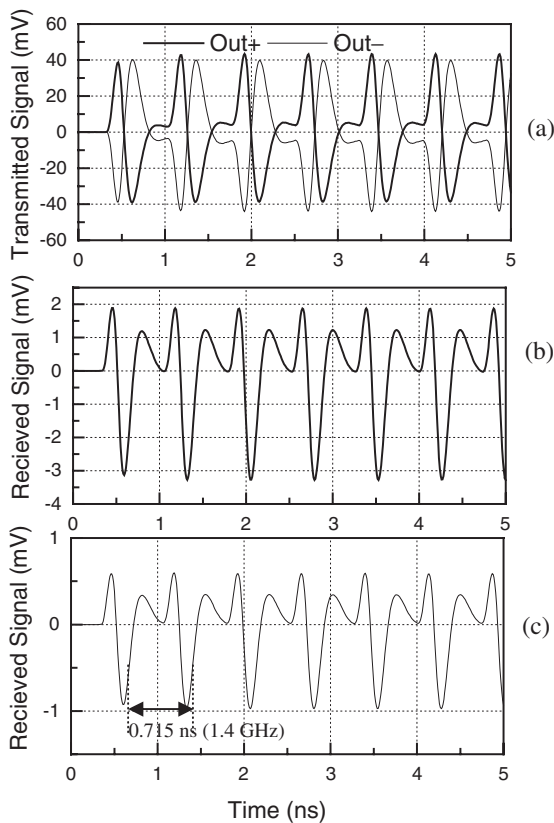

Fig. 14. GMP transmission using integrated antennas in silicon. (a) Transmitted signal. (b) Received signal for $d = 1$ mm. (c) Received signal for $d = 3$ mm. The receiving antenna was terminated with a 100-Ω load for different communication distances.

Table I. Performance data for differential Gaussian monocycle pulse generator.

Output	Differential GMP
GMP peak to peak amplitude (mV)	152
GMP center frequency (GHz)	2.4
3-dB bandwidth (GHz)	2.8
Power consumption at 1.8 V (mW)	44
Pulse repetition rate (GHz)	1.4
Maximum data transmission rate (Gbps)	1.4
Chip area (excluding antenna) (mm^2)	0.06
Technology	TSMC 0.18 μm CMOS

mission and reception of DGMP by a 6-mm-long integrated dipole antenna pair in silicon for intrachip communication is confirmed by simulation. The simulation showed that the DGMP repetition rate is 1.4 GHz; thus, a data transmission rate of 1.4 Gbps could be achieved. In this study, a 6-mm-long dipole antenna occupies a large area on the silicon. This area can be scaled down in future ULSI by generating DGMPs with high center frequency. In future ULSIs, device size will be scaled down from 180 to 32 nm, and the Gaussian monocycle pulse center frequency may be increased to 30 GHz by generating a triangular shaped pulse with fast rise and fall times in a 32 nm CMOS process. Consequently the antenna length will be scaled down from 6 to 1 mm.

Acknowledgements

1) K. Kanda, D. D. Antono, K. Ishida, H. Kawaguchi, T. Kuroda and Sakurai: ISSCC Dig. Tech. Pap., 2003, p. 186.
2) D. Mizoguchi, Y. B. Yusof, N. Miura, T. Sakurai and T. Kuroda: ISSCC Dig. Tech. Pap., 2004, p. 142.
3) A. B. M. H. Rashid, S. Watanabe and T. Kikkawa: IEEE Electron Device Lett. **23** (2002) 731.
4) B. Sklar: *Digital Communications Fundamentals and Applications* (Addison-Wesley Longman, Singapore, 2001) 2nd ed., Chap. 12, p. 718.
5) M. Z. Win and R. A. Scholtz: IEEE Commun. Lett. **2** (1998) 36.
6) J. Han and C. Nguyen: IEEE Microwave Wireless Components Lett. **12** (2002) 206.
7) P. K. Saha, N. Sasaki and T. Kikkawa: Jpn. J. Appl. Phys. **44** (2005) 2104.
8) HSPICE User's Manual, Meta-Software, Inc., U.S.A., 1996.
9) CST Microwave Studio®, ver. 5, AET Japan, 2004.
10) S. Watanabe, K. Kimoto and T. Kikkawa: Proc. IEEE-APS Int. Symp. USNC/URSI National Radio and Science Meet., 2004, p. 2277.
11) EMtoSPICE converter, EM Wonder, U.S.A.